AIAA JOURNAL
Vol. 33, No. 11, November 1995

Prediction of Nonequilibrium Turbulent Flows with Explicit Algebraic Stress Models

Ridha Abid*
High Technology Corporation, Hampton, Virginia 23666
and
Christopher Rumsey† and Thomas Gatski‡
NASA Langley Research Center, Hampton, Virginia 23681-0001

An explicit algebraic stress equation, developed by Gatski and Speziale, is used in the framework of the K-ω and K-ε formulations to predict two-dimensional separated turbulent flows. The nonequilibrium effects are modeled through coefficients that depend nonlinearly on both rotational and irrotational strains. The proposed models were implemented in the Courant–Friedrichs–Lewy three-dimensional Navier–Stokes code. Comparisons with the experimental data are presented, which clearly demonstrate that explicit algebraic stress models improve the response of standard two-equation models to nonequilibrium effects.

I. Introduction

COMPUTATIONAL fluid dynamics has become an increasingly powerful tool in the aerodynamic design of aerospace vehicles as a result of improvements in numerical algorithms and computer capabilities (e.g., speed, storage). Major future gains in efficiency are expected to come about as massively parallel supercomputer technology matures. However, some critical pacing items limit the effectiveness of computational fluid dynamics in engineering. Chief among these items is turbulence modeling. Several turbulence models of varying degrees of complexity, which can be classified as either eddy viscosity or Reynolds stress models, have been proposed. Excellent reviews of turbulence models have been provided by both Speziale[1] and Wilcox.[2]

Eddy viscosity models use the Boussinesq isotropic effective viscosity concept, which assumes that the turbulent stresses in the mean momentum equation are equal to the product of an eddy viscosity and a mean strain rate. Zero-, one-, and two-equation models are among the most popular eddy viscosity models for engineering applications because of their ease of implementation in computational fluid dynamics codes. Algebraic or zero-equation models, which assume local equilibrium of the turbulent and mean flow, have provided reasonable predictions for simple flows. When the turbulent transport is important or the mean conditions change abruptly, these models do not work well. One-equation models improve the predictions for simple near-equilibrium flows but do not account for complex effects on turbulence. Two-equation models are developed to take explicit account of the history of the turbulence through two transport equations for turbulent length and time scales. These models offer good predictions of the characteristics and physics of simple separated flows and flows with gradual changes in boundary conditions. However, two-equation models fail in many practical flows because they cannot properly account for streamline curvature, rotational strains and buoyancy; they provide an incorrect response to strong adverse pressure gradients; and they cannot describe the anisotropy of turbulence. As a result, various ad hoc modifications to the models have been proposed to achieve the proper response (see Lakshminarayana[3]). In these modifications, effects on turbulence, such as those due to streamline curvature, have been directly accounted for in the eddy viscosity expression or have been reflected indirectly in the turbulence-model equations by modifying the dissipation-rate equation. The improved two-equation models predict a wider range of flows; however, they still fail to properly capture the physics in a broad class of flows. To overcome some of these deficiencies, two-equation turbulence models that are nonlinear in the mean strain rate were proposed by Speziale[4] and Rubinstein and Barton.[5] These models have provided accurate predictions of turbulence intensities. However, these models are not consistent with Reynolds stress models because they have constant coefficients.

Reynolds stress models represent the highest level of closure that is currently feasible for practical calculations. These models are superior to the two-equation models in that they eliminate the assumption that the turbulent stresses respond immediately to changes in the mean strain rate. Also, they account for the anisotropy of turbulence and some extra effects on turbulence (e.g., due to streamline curvature and rotation) through extra production terms that explicitly appear in the Reynolds stress transport equation. However, models for many unknown turbulent quantities are required. This need is generally met by assuming that the turbulence is locally homogeneous and in equilibrium. Existing Reynolds stress models have been shown to give good descriptions of two-dimensional mean turbulent flows that are near equilibrium. However, computer costs and numerical stability problems that arise from the absence of the turbulent viscosity make assessment of the limitations of these models in predicting complex flows difficult. However, second-order closure models could be used to derive better two-equation models because fundamentally they are constructed on a stronger theoretical basis than the lower level models.

Recently, a methodology for deriving a general nonlinear constitutive relation (or an explicit algebraic stress equation) for the Reynolds stress tensor from second-order closures has been proposed by Gatski and Speziale,[6] based on the ideas of Pope.[7] This derivation is based on the assumptions that the net convection of the turbulent stresses is proportional to the net convection of the turbulent kinetic energy and that the structural parameters of the turbulence are constant along a streamline. As a result, a new generation of two-equation models is obtained with coefficients that depend on rotational and irrotational strains. This new feature extends the range of applicability of the standard two-equation models.

In this paper, the algebraic stress equation is applied within the context of the K-ω and K-ε two-equation models. The ability of the proposed models to predict nonequilibrium flows is evaluated systematically, including transonic flow over an axisymmetric bump and flow over two different airfoils. The Courant–Friedrichs–Lewy three-dimensional (CFL3D) Navier–Stokes code is used to simulate the flows considered.

Received Feb. 6, 1995; revision received May 4, 1995; accepted for publication May 11, 1995.

*Senior Research Scientist. Member AIAA.
†Research Scientist. Member AIAA.
‡Senior Research Scientist.

II. Theoretical Analysis

For a weakly compressible turbulent flow at high Reynolds numbers, the Reynolds stress tensor $\tau_{ij} = \overline{u_i u_j}$ is a solution of the transport equation[8]

$$\frac{D\tau_{ij}}{Dt} = -\tau_{ik}\frac{\partial \bar{u}_j}{\partial x_k} - \tau_{jk}\frac{\partial \bar{u}_i}{\partial x_k} + \frac{\Pi_{ij}}{\bar{\rho}} - \frac{2}{3}\varepsilon\delta_{ij} + D_{ij}^T + \nu\nabla^2\tau_{ij} \quad (1)$$

given that Π_{ij} is the pressure-strain correlation, D_{ij}^T is the turbulent transport term, ε is the turbulent dissipation rate, ν is the kinematic viscosity, $\bar{u}_i$ is the mean-velocity component, $\bar{\rho}$ and is the mean density. Explicit compressibility effects are neglected in Eq. (1) due to the applicability of Markovin's hypothesis in these weakly compressible flows.

If we contract the indices in Eq. (1), then we obtain the transport equation for the turbulent kinetic energy $K = \overline{u_i u_i}/2$:

$$\frac{DK}{Dt} = P - \varepsilon + D_K^T + \nu\nabla^2 K \quad (2)$$

given that $P = -\tau_{ij}(\partial \bar{u}_i/\partial x_j)$ is the turbulence production term and D_K^T is the turbulent transport term.

Rodi[9] proposed the idea of algebraic stress closure, which provides algebraic equations without solving differential equations for the Reynolds stresses. He assumed that

$$\frac{D\tau_{ij}}{Dt} - \nu\nabla^2\tau_{ij} - D_{ij}^T = \frac{\tau_{ij}}{K}\left(\frac{DK}{Dt} - D_K^T - \nu\nabla^2 K\right) \quad (3)$$

and

$$\frac{Db_{ij}}{Dt} = 0 \quad (4)$$

where

$$b_{ij} = \frac{\tau_{ij} - \frac{2}{3}K\delta_{ij}}{2K} \quad (5)$$

is the anisotropic Reynolds stress. Physically, two assumptions are made in the algebraic Reynolds stress closures: the convection term minus the diffusion term in the Reynolds stress equation is proportional to the convection term minus the diffusion term in the turbulent kinetic energy equation and the anisotropic Reynolds stress b_{ij} is constant along a streamline.

The substitution of Eqs. (3) and (4) into Eq. (1) yields the following algebraic stress equation:

$$(P-\varepsilon)b_{ij} = -\tfrac{2}{3}KS_{ij} - K\left(b_{ik}S_{jk} + b_{jk}S_{ik} - \tfrac{2}{3}b_{mn}S_{mn}\delta_{ij}\right) - K(b_{ik}W_{jk} + b_{jk}W_{ik}) + (\Pi_{ij}/2\bar{\rho}) \quad (6)$$

where

$$S_{ij} = \frac{1}{2}\left(\frac{\partial \bar{u}_i}{\partial x_j} + \frac{\partial \bar{u}_j}{\partial x_i}\right) \quad (7)$$

and

$$W_{ij} = \frac{1}{2}\left(\frac{\partial \bar{u}_i}{\partial x_j} - \frac{\partial \bar{u}_j}{\partial x_i}\right) \quad (8)$$

are the mean-rate-of-strain tensor and mean-vorticity tensor, respectively.

Given a pressure-strain-correlation model, Eq. (6) provides an implicit algebraic equation for the determination of the Reynolds stress τ_{ij}. Computations that use this model have shown that stable numerical solutions are difficult to obtain. Hence, an explicit algebraic stress equation that is a mathematically consistent representation of Eq. (6) is preferable.

Pope[7] developed a methodology for obtaining explicit algebraic stress equations by using a tensorial polynomial expansion in an integrity basis. Gatski and Speziale[6] used this method to derive an explicit algebraic stress equation for three-dimensional turbulent flows. To generalize their results, they applied their algebraic stress representation to the general class of pressure-strain-correlation models for Π_{ij} that are linear in the anisotropic tensor b_{ij}. The general form of Π_{ij} is

$$(\Pi_{ij}/\bar{\rho}) = -C_1\varepsilon b_{ij} + C_2 K S_{ij} + C_3 K\left(b_{ik}S_{jk} + b_{jk}S_{ik} - \tfrac{2}{3}b_{mn}S_{mn}\delta_{ij}\right) + C_4 K(b_{ik}W_{jk} + b_{jk}W_{ik}) \quad (9)$$

The explicit nonlinear constitutive equation, derived by Gatski and Speziale,[6] is then given after regularization by

$$\bar{\rho}\tau_{ij} = \tfrac{2}{3}\bar{\rho}K\delta_{ij} - 2\mu_t\left[\left(S_{ij} - \tfrac{1}{3}S_{kk}\delta_{ij}\right) + (\alpha_4/\omega)(S_{ik}W_{kj} + S_{jk}W_{ki}) - (\alpha_5/\omega)\left(S_{ik}S_{kj} - \tfrac{1}{3}S_{kl}S_{kl}\delta_{ij}\right)\right] \quad (10)$$

with

$$\mu_t = \bar{\rho}C_\mu^*(K/\omega) \quad (11)$$

$$C_\mu^* = \frac{3(1+\eta^2)\alpha_1}{3 + \eta^2 + 6\eta^2\xi^2 + 6\xi^2} \quad (12)$$

$$\eta^2 = (\alpha_2/\omega^2)(S_{ij}S_{ij}), \qquad \xi^2 = (\alpha_3/\omega^2)(W_{ij}W_{ij}) \quad (13)$$

where $\bar{\rho}$ is the mean density and $\omega = \varepsilon/K$ is the specific dissipation rate. The constants in Eqs. (11–13) are given by

$$\alpha_1 = \left(\tfrac{4}{3} - C_2\right)(g/2), \qquad \alpha_2 = (2 - C_3)^2(g^2/4) \quad (14)$$

$$\alpha_3 = (2 - C_4)^2(g^2/4), \qquad \alpha_4 = \left(\frac{2 - C_4}{2}\right)g \quad (15)$$

$$\alpha_5 = (2 - C_3)g, \qquad g = \frac{1}{(C_1/2) + C_5 - 1} \quad (16)$$

Note that the derivation of Eq. (10) is valid for both the K-ω and K-ε formulations. In the present study, the pressure-strain-correlation model of Launder et al.[10] is considered; the coefficients are

$$C_1 = 3, \quad C_2 = 0.8, \quad C_3 = 1.75, \quad C_4 = 1.31, \quad C_5 = 2 \quad (17)$$

The nonlinear constitutive equation (10) must be solved in conjunction with two transport equations. Therefore, two models will be proposed. In model A, the K and ω equations are solved with Eq. (10); in model B, the K and ε equations are solved with Eq. (10).

Model A

The modeled transport equations for K and ω are

$$\bar{\rho}\frac{DK}{Dt} = \bar{\rho}P - \bar{\rho}\omega K + \frac{\partial}{\partial x_j}\left(\frac{\mu_{tl}}{\sigma_k}\frac{\partial K}{\partial x_j}\right) \quad (18)$$

and

$$\bar{\rho}\frac{D\omega}{Dt} = C_{\omega_1}\bar{\rho}\frac{\omega}{K}P - C_{\omega_2}\bar{\rho}\omega^2 + \frac{\partial}{\partial x_j}\left(\frac{\mu_{tl}}{\sigma_\omega}\frac{\partial \omega}{\partial x_j}\right) \quad (19)$$

given that $\mu_{tl} = C_{\mu l}^*\bar{\rho}(K/\omega)$ and that $C_{\mu l}^*$ ($= 0.088$) is the value of C_μ^* in the logarithmic layer. The coefficients of the model are

$$\sigma_k = 1.4, \quad \sigma_\omega = 2.0, \quad C_{\omega_2} = 0.83, \quad \kappa = 0.41 \quad (20)$$

and

$$C_{\omega_1} = C_{\omega_2} - \frac{\kappa^2}{\sqrt{C_{\mu l}^*}\sigma_\omega} \quad (21)$$

The coefficient C_{ω_1} was chosen so that the equation for ω satisfies the law of the wall. The model A will be compared with the isotropic K-ε model of Wilcox[11] (hereafter referred to as WL), which has the following coefficients:

$$\sigma_k = 2, \qquad \sigma_\omega = 2, \qquad C_{\omega_2} = 0.83, \qquad \kappa = 0.41 \tag{22}$$

and

$$C_\mu^* = C_{\mu l}^* = 0.09 \tag{23}$$

Note that the Wilcox model uses the Boussinesq eddy viscosity concept ($\alpha_4 = \alpha_5 = 0$) and has a constant value for C_μ^*.

At the wall, the boundary conditions for K and ω, as suggested by Menter,[12] are

$$K = 0, \qquad \omega = 10\frac{6\nu}{C_{\omega_2}(\Delta y)^2} \tag{24}$$

where Δy is the distance to the first cell center away from the wall.

Model B

The modeled transport equations for K and ε are

$$\bar{\rho}\frac{DK}{Dt} = \bar{\rho}P - \bar{\rho}\varepsilon + \frac{\partial}{\partial x_j}\left(\frac{\mu_{tl}}{\sigma_k}\frac{\partial K}{\partial x_j}\right) \tag{25}$$

and

$$\bar{\rho}\frac{D\varepsilon}{Dt} = C_{\varepsilon_1}\bar{\rho}\frac{\varepsilon}{K}P - C_{\varepsilon_2}\bar{\rho}f\frac{\varepsilon^2}{K} + \frac{\partial}{\partial x_j}\left(\frac{\mu_{tl}}{\sigma_\varepsilon}\frac{\partial \varepsilon}{\partial x_j}\right) \tag{26}$$

given that $\mu_{tl} = C_{\mu l}^*\bar{\rho}(K^2/\varepsilon)$ and $C_{\mu l}^*$ ($= 0.088$) is the value of C_μ^* in the logarithmic layer. The coefficients of the model are

$$\sigma_k = 1.0, \qquad \sigma_\varepsilon = 1.3, \qquad \kappa = 0.41, \qquad C_{\varepsilon_2} = 1.83 \tag{27}$$

$$C_{\varepsilon_1} = C_{\varepsilon_2} - \frac{\kappa^2}{\sqrt{C_{\mu l}^*}\sigma_\varepsilon} \tag{28}$$

and

$$f = \left[1 - \exp\left(-\frac{y^+}{6.4}\right)\right]^2, \qquad y^+ = \frac{yu_\tau}{\nu} \tag{29}$$

or

$$f = \left[1 - \exp\left(-\frac{R_y}{12.5}\right)\right], \qquad R_y = \frac{\sqrt{K}y}{\nu} \tag{30}$$

given that u_τ is the shear velocity and y is normal to the wall. Note that model B can be integrated directly to the wall without adding a damping to the eddy viscosity. The function f is introduced to remove the singularity of the dissipation equation at the wall. This idea was introduced by Speziale and Abid.[13]

At the wall, the boundary conditions for K and ε are

$$K = 0, \qquad \varepsilon = 2\nu\left(\frac{\partial\sqrt{K}}{\partial y}\right)^2 \tag{31}$$

Model B will be compared with the isotropic eddy viscosity model developed by Abid[14] (hereafter referred to as AB) for transitional and turbulent flows. The model has the following coefficients:

$$\sigma_k = 1.0, \qquad \sigma_\varepsilon = 1.4, \qquad C_{\varepsilon_1} = 1.45, \qquad C_{\varepsilon_2} = 1.83 \tag{32}$$

The AB model uses the Boussinesq eddy viscosity concept ($\alpha_4 = \alpha_5 = 0$) and has the following relations for C_μ^* and f:

$$C_\mu^* = C_{\mu l}^*\tanh(0.008R_y)\left(1 + \frac{4}{R_t^{\frac{3}{4}}}\right) \tag{33}$$

and

$$f = 1 - \exp\left(-\frac{R_y}{12}\right) \tag{34}$$

where $C_{\mu l}^* = 0.09$ and $R_t = K^2/\nu\varepsilon$ is the turbulent Reynolds number.

In the turbulence-model equations, the production term P is approximated in the standard two-equations models (WL and AB models) as $2\nu_t W_{ij}W_{ij}$. This approximation is often used for many airfoil type of aerodynamic flow computations with little effect on the results.

The new nonlinear constitutive relationship for the Reynolds stress tensor [Eq. (10)], which extends the range of validity for the standard two-equation model, has two important features. First, the new explicit algebraic equation can account for the anisotropy of the Reynolds stresses and, therefore, can predict turbulent-driven secondary flows. In fact, the equilibrium Reynolds stress anisotropies in homogeneous shear flow or in the log layer of channel flow, which are derived from Eq. (10), are given by

$$b_{11} = \left(\frac{\alpha_4}{2} + \frac{\alpha_5}{12}\right)\frac{P}{\varepsilon} \tag{35}$$

$$b_{22} = \left(-\frac{\alpha_4}{2} + \frac{\alpha_5}{12}\right)\frac{P}{\varepsilon} \tag{36}$$

$$b_{33} = -\frac{\alpha_5}{6}\frac{P}{\varepsilon} \tag{37}$$

and

$$b_{12} = -\frac{1}{2(\Gamma K/\varepsilon)}\frac{P}{\varepsilon} \tag{38}$$

with $\Gamma = (2S_{ij}S_{ij})^{1/2}$. These equilibrium values are very close to those obtained with the full Reynolds stress model. When the Launder et al. pressure-strain-correlation model is used, the magnitude of the normal Reynolds stress anisotropies are underpredicted. This deficiency is due to the inaccurate calibration of the Launder et al. model for homogeneous shear flow, as shown by Abid and Speziale.[15] An explicit algebraic stress equation will correctly predict the anisotropy of the Reynolds stress if the pressure-strain-correlation model is calibrated to yield good equilibrium values for homogeneous shear flows. The Speziale et al. model[6] is more accurately calibrated but is not used in this study because it shows evidence of numerical instability in the context of the algebraic stress formulation when the flow is far from equilibrium (i.e., $\Gamma K/\varepsilon$ is large). This is because the model responds more sensitively to rotational strains. Systematically derived nonequilibrium extensions of the model are currently under investigation that appear to remedy this problem.

Second, the explicit algebraic stress model improves the ability of two-equation models to account for nonequilibrium effects through the coefficient C_μ^*. To illustrate this point, we consider two-dimensional turbulent thin shear layers. In this case, the coefficient

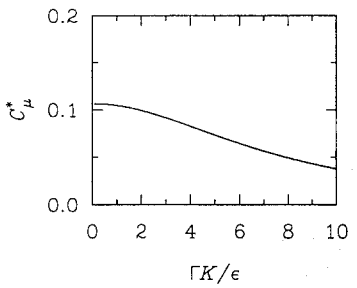

Fig. 1 Distribution of C_μ^* vs parameter $\Gamma K/\varepsilon$.

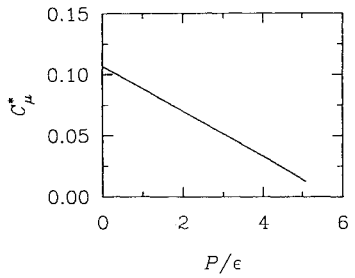

Fig. 2 Distribution of C_μ^* vs parameter P/ε.

C_μ^* depends on the shear parameter $\Gamma K/\varepsilon$ or the parameter P/ε through the relation

$$(P/\varepsilon) = C_\mu^*(\Gamma K/\varepsilon)^2 \tag{39}$$

Figures 1 and 2 clearly show that the coefficient C_μ^* (and therefore the eddy viscosity) decreases as the parameter $\Gamma K/\varepsilon$ as the effects of an increase or adverse pressure gradient increase. This finding is consistent with experimental findings.

III. Results and Discussion

The calculations to be presented were done with the three-dimensional thin-layer Navier–Stokes CFL3D code,[16] which uses a second-order-accurate finite volume scheme. The convective terms are discretized with an upwind scheme that is based on Roe's flux-difference splitting method. All viscous terms are centrally differenced. The equations are integrated in time with an implicit, spatially split approximate-factorization scheme.

The thin-layer approximation retains only those viscous terms with derivatives normal to the body surface. It is generally considered to be a good approximation for high-Reynolds-number aerodynamic flows with little separation. The thin-layer assumption is also used for all $\partial\bar{u}_i/\partial\bar{x}_j$ terms appearing in the source terms of the turbulent equations. The effects of grid density have been assessed in previous studies using the CFL3D code (see Refs. 12 and 15) and are not repeated here.

The performance of the turbulence models selected in the present study was evaluated for the flat-plate turbulent boundary layer at a zero pressure gradient. As expected (the results are not shown here), all turbulence models yielded good predictions of the mean-velocity profiles and skin-friction coefficients. Note that the turbulent algebraic stress model within the context of the K-ε formulation (model B) can be integrated directly to a solid boundary with no damping function in the turbulent eddy viscosity. Although some turbulence properties near the wall are not captured (i.e., the peak of the turbulent kinetic energy), model B does give accurate results away from the buffer layer (i.e., $y^+ > 40$).

The first case to be considered is the supercritical airfoil RAE 2822 (case 9), which was tested by Cooke et al.[17] The airfoil has a maximum thickness of 12.1% c and a leading-edge radius of 0.827% c (c is the chord of the airfoil).

The grid used is a $257 \times 97\,C$ mesh with 177 points on the airfoil and a minimum spacing at the wall of $0.932 \times 10^{-6}c$. The outer boundary extent is approximately $18c$, and transition is assumed at 3% c. For case 9, the conditions include a Mach number $M_\infty = 0.73$, an angle of attack $\alpha = 2.8$ deg, and a Reynolds number $Re = 6.5 \times 10^6$.

This case contains no separated flow and is not, therefore, particularly challenging. However, such building block flows need to be considered in validating turbulence models to provide a complete picture of this range of applicability. Figures 3 and 4 compare the surface pressure coefficients computed along the airfoil surface from the four turbulence models with the experimental data. Those models based on the K-ω formulation provide a good representation of the pressure over most of the airfoil. On the other hand, the models based on the K-ε formulation predict a shock location that is upstream of the location shown in the experiment.

The skin-friction coefficients along the airfoil surface for the four models are compared with the experimental results in Figs. 5 and 6.

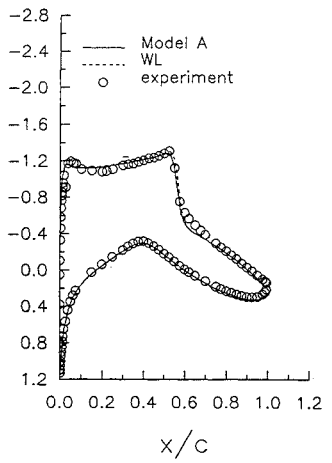

Fig. 3 Surface pressure distribution for RAE 2822 (case 9).

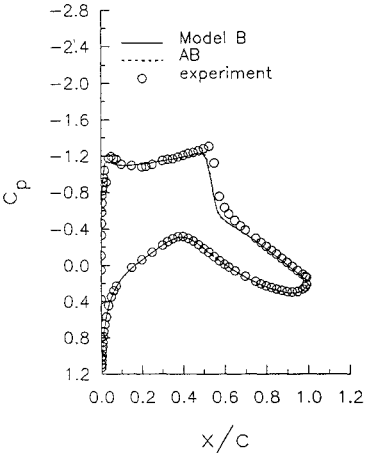

Fig. 4 Surface pressure distribution for RAE 2822 (case 9).

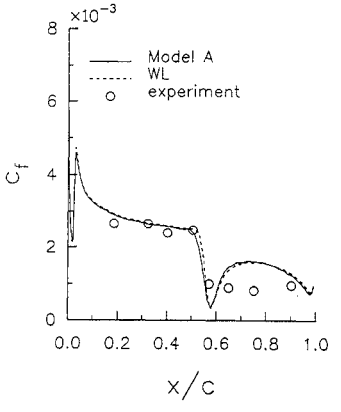

Fig. 5 Skin-friction coefficient for RAE 2822 (case 9).

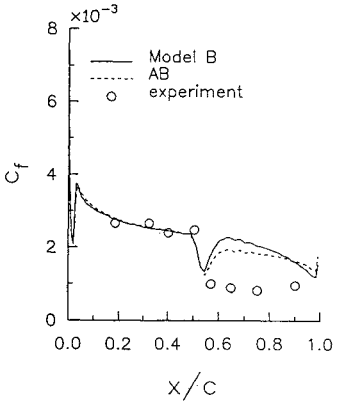

Fig. 6 Skin-friction coefficient for RAE 2822 (case 9).

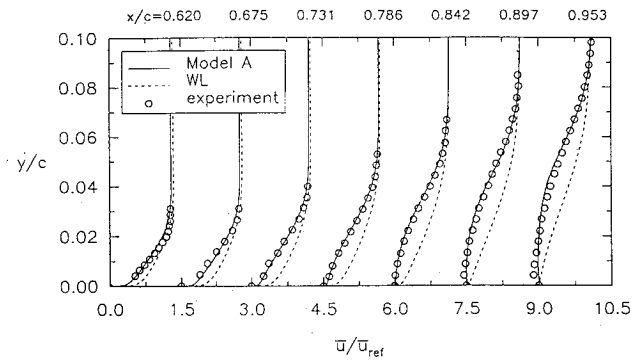

Fig. 7 Mean-velocity profiles for NACA 4412.

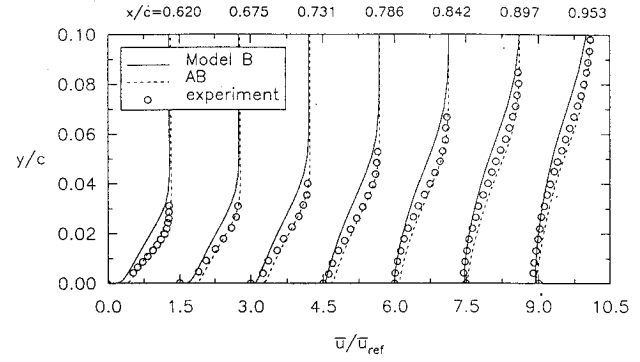

Fig. 8 Mean-velocity profiles for NACA 4412.

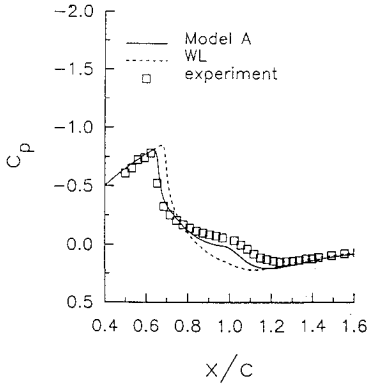

Fig. 9 Surface pressure distribution for transonic bump flow.

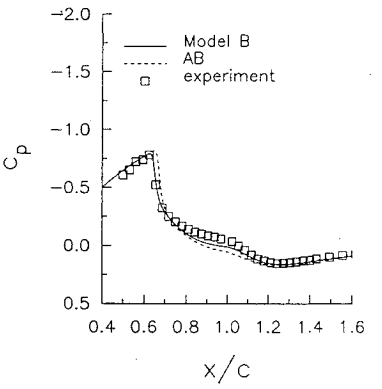

Fig. 10 Surface pressure distribution for transonic bump flows.

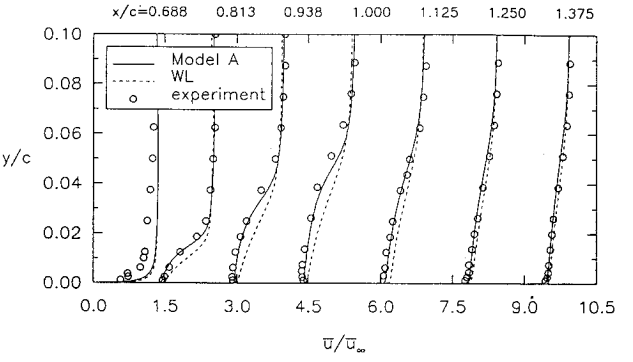

Fig. 11 Mean-velocity profiles for transonic bump flow.

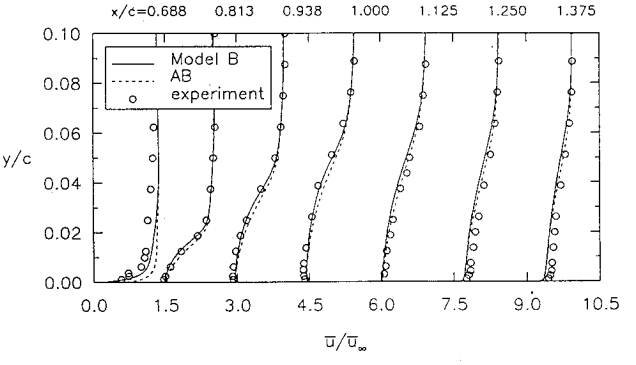

Fig. 12 Mean-velocity profiles for transonic bump flow.

All models overpredict the skin-friction coefficient downstream of the shock; however, the models using the K-ε formulation predict levels that are unrealistically high. This deficiency results from the tendency of the K-ε models to predict excessive near-wall levels of turbulent length scale in the presence of an adverse pressure gradient, which leads to high values of the eddy viscosity.

The second case to be considered is the NACA 4412 airfoil experiment of Coles and Wadcock.[18] This case involves separation and, therefore, is more challenging than the previous case. The experiment was conducted at the following conditions: $Re = 1.52 \times 10^6$, based on the chord length; $M_\infty = 0.2$; and $\alpha = 13.87$ deg. The grid used was $257 \times 97C$ mesh with 177 points on the airfoil, a minimum spacing at the wall of $0.227 \times 10^{-4}c$, and an outer boundary extent of approximately $18c$. It should be noted that the wind-tunnel walls probably need to be modeled in the computation to account for their effect on the surface pressures. However, the velocity profiles from this case using a "free air" grid have been used so often to validate turbulence models that we include them here for completeness and consistency with previous studies. Although outside the scope of the present study, turbulent model validation utilizing this case in an external flow geometry should be redone in the more precise internal flow configuration. Figures 7 and 8 compare the computed mean-velocity profiles at different stations with the experimental data. As shown in Figs. 7 and 8, the nonequilibrium effects for this case are significant, and the solution obtained with the WL model predicts too little separation; results from model A agree well with the data. Model B predicts too much separation; model AB gives surprisingly satisfactory results.

The third case to be considered is a transonic flow over an axisymmetric bump.[19] This flow was developed over an axisymmetric hollow cylinder that was aligned with the flow direction. A circular arc bump was used to develop a strong shock to induce separation. The separation occurred at $x/c = 0.7$, and the flow reattached at $x/c = 1.15$ (x/c is the distance from the leading edge of the circular arc section). A $181 \times 101 \times 2$ grid was used with 88 points on the bump and a minimum spacing at the wall of $0.198 \times 10^{-4}c$. The upper boundary is approximately $3.7c$ above the bump.

In Figs. 9 and 10, the experimental surface pressure distributions for $M_\infty = 0.875$ and $Re = 2.66 \times 10^6$ are compared with computed profiles obtained from the four different turbulence models. As shown in Figs. 9 and 10, the surface pressure distributions obtained with turbulence models based on the algebraic stress equation are in better agreement with the experimental results than those obtained with either the WL or the AB model. Models A and B show some improvement in establishing both the location of the shock and the pressure level in the vicinity of separation.

The computed velocity and Reynolds shear stress profiles are compared with the experimental results in Figs. 11–14. The profiles predicted by the models based on the algebraic stress equation agree better with the experimental data than those predicted by the AB

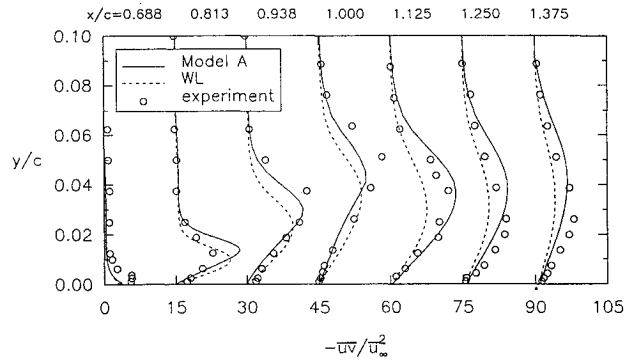

Fig. 13 Turbulent shear stress profiles for transonic bump flows.

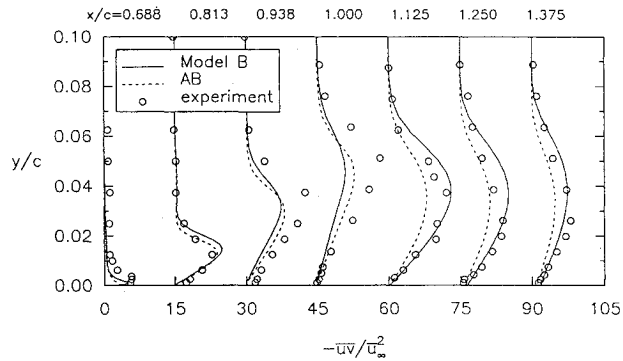

Fig. 14 Turbulent shear stress profiles for transonic bump flows.

and WL turbulence models. This result is due to the ability of the algebraic stress models to limit the rise of the Reynolds shear stress in the vicinity of the shock. As evident from Fig. 2, the coefficient C_μ^* decreases when the parameter P/ε increases in adverse-pressure-gradient flows, which results in the reduction of the eddy viscosity and, therefore, of the turbulent shear stress. Additionally, model A performs well in predicting mean-velocity profiles in the pressure recovery region downstream of the reattachment ($x/c > 1.15$). However, model B does not perform as well in this region.

IV. Conclusions

A study of explicit algebraic stress models, used in the framework of the K-ε and K-ω formulations for separated turbulent flows, has been conducted. This new generation of two-equation models, which is derived from second-order closures, has been tested against three test cases, two of which involve separation. The linear pressure-strain-correlation model of Launder et al. was selected in this study. Two major findings have been made in this study: explicit algebraic stress models have shown some improvement over the standard two-equation models because of their ability to account for nonequilibrium effects and explicit algebraic stress models can be integrated to a solid boundary with no damping function in the turbulent eddy viscosity. Thus the explicit algebraic stress formulation increased the range of applicability of a two-equation turbulent closure formulation at a minimal increase in cost and storage. Further study is needed to select the pressure-strain-correlation model that provides the correct response to complex effects such as rotational and anisotropic effects.

Acknowledgment

The first author would like to thank NASA Langley Research Center for support under Contract NAS1-19299.

References

[1]Speziale, C. G., "Analytical Methods for the Development of Reynolds Stress Closures in Turbulence," *Annual Review of Fluid Mechanics*, Vol. 23, 1991, pp. 107–157.

[2]Wilcox, D. C., *Turbulence Modeling for CFD*, DCW Industries, Inc., La Cañada, CA, 1993.

[3]Lakshminarayana, B., "Turbulence Modelling for Complex Flows," AIAA Paper 85-1652, 1985.

[4]Speziale, C. G., "On Nonlinear K-l and K-ε Models of Turbulence," *Journal of Fluid Mechanics*, Vol. 178, 1987, p. 459.

[5]Rubinstein, R., and Barton, J. M., "Nonlinear Reynolds Stress Models and the Normalization Group," *Physics of Fluids*, Vol. A2, 1990, p. 1472.

[6]Gatski, T. B., and Speziale, C. G., "On Explicit Algebraic Stress Models for Complex Turbulent Flows," *Journal of Fluid Mechanics*, Vol. 254, 1993, pp. 59–78.

[7]Pope, S. B., "A More General Effective Viscosity Hypothesis," *Journal of Fluid Mechanics*, Vol. 72, 1975, pp. 331–340.

[8]Hinze, J. O., *Turbulence*, McGraw–Hill, New York, 1975.

[9]Rodi, W., "A New Algebraic Relation for Calculation the Reynolds Stresses," *Zeitschrift für Angewandte Mathematik und Mechanik*, Vol. 56, 1976, pp. T219–T221.

[10]Launder, B. E., Reece, G. J., and Rodi, W., "Progress in the Development of a Reynolds Stress Turbulence Closure," *Journal of Fluid Mechanics*, Vol. 68, 1975, pp. 537–566.

[11]Wilcox, D. C., "Reassessment of the Scale Determining Equation for Advanced Turbulence and Models," *AIAA Journal*, Vol. 26, 1988, pp. 1299–1310.

[12]Menter, F. R., and Rumsey, C. L., "Assessment of Two-Equation Turbulence Models for Transonic Flows," AIAA Paper 94-2343, 1994.

[13]Speziale, C. G., and Abid, R., "Towards the Near-Wall Integration of Reynolds Stress Turbulence Closures with No Wall Damping," *AIAA Journal*, Vol. 33, No. 10, 1995, pp. 1974–1977.

[14]Abid, R., "Evaluation of Two-Equation Turbulence Models for Predicting Transitional Flows," *International Journal of Engineering Sciences*, Vol. 31, 1993, pp. 831–840.

[15]Abid, R., and Speziale, C. G., "Predicting Equilibrium States with Reynolds Stress Closures in Channel Flow and Homogeneous Shear Flow," *Physics of Fluids A* , Vol. 5, No. 7, 1993, pp. 1776–1782.

[16]Rumsey, C. L., and Vatsa, V. N., "A Comparison of the Predictive Capabilities of Several Turbulence Models Using Upwind and Central-Difference Computer Codes," AIAA Paper 93-0192, 1993.

[17]Cooke, P., McDonald, M., and Firmin, M., "Airfoil RAE2822—Pressure Distributions and Boundary Layer Wake Measurements," AGARD AR-138, 1979.

[18]Coles, D., and Wadcock, A. J., "Flying-Hot-Wire Study of Flow Past an NACA 4412 Airfoil at Maximum Lift," *AIAA Journal*, Vol. 17, No. 4, 1979.

[19]Bachalo, W. D., and Johnson, D. A., "An Investigation of Transonic Turbulent Boundary Layer Separation Generated on an Axisymmetric Flow Model," AIAA Paper 79-1479, 1979.